Journal of Physics:
Conference Series

PAPER • **OPEN ACCESS**

In situ measurements of near wake dynamics with a fleet of multicopter drones

To cite this article: Norman Wildmann and Johannes Kistner 2025 *J. Phys.: Conf. Ser.* **3016** 012011

Journal of Physics: Conference Series **3016** (2025) 012011 doi:10.1088/1742-6596/3016/1/012011

In situ measurements of near wake dynamics with a fleet of multicopter drones

Norman Wildmann[1], **Johannes Kistner**[1]

[1]Deutsches Zentrum für Luft- und Raumfahrt e.V., Institut für Physik der Atmosphäre, Oberpfaffenhofen, Germany

E-mail: norman.wildmann@dlr.de

Abstract. This study presents an analysis of wind turbine near wake vortices using a fleet of multicopter drones. Motivated by the need for accurate wake modeling for wind farm optimization, particularly in closely spaced layouts and repowering scenarios, the research addresses the limited availability of full-scale wake vortex data. While previous studies have employed numerical models, wind tunnel experiments, and single drone measurements, this work focuses on analyzing a larger dataset of in situ measurements. A methodology for automatic vortex detection and parameter extraction (circulation and core radius) from the drone fleet data is developed and applied to more than 300 observed vortices. The results demonstrate the feasibility of measuring vortex decay with this approach, indicating an expected increase in core radius with vortex age. The study also highlights the challenges and uncertainties associated with the method. Improvements are suggested for the future to locate drones slightly outside the expected wake area and in more streamwise distances downstream.

1 Introduction

The optimization of existing and future wind parks is a key challenge for competitiveness of wind energy. Mitigating the negative impacts of wakes in staggered layouts through design, siting and control requires accurate modeling. For optimal land-use, especially considering repowering of wind farms, wind turbines may be facing smaller relative distances in future and thus be subject to coherent vortices of upstream turbines. Reduced turbine spacing and potential impact of near wake turbulence can lead to increased fatigue loading [1]. A recent study by Neunaber et al. [2] also highlighted the importance of defining a virtual origin of the far wake in common engineering wake models, which is closely connected to near wake dynamics. The near wake is characterized by tip vortices that propagate downstream, interact with ambient turbulence and thus decay. This process has been studied in the past using numerical models [3, 4] or wind tunnel experiments [5, 6, 7]. Very limited data of full-scale wind turbine wake vortices are available. Meteorological masts cannot easily be placed close enough to the turbines and lidar remote sensing does not have the necessary resolution or requires scanning solutions that depend on assumptions of flow stationarity. Recently, drones have been deployed to measure in situ in wind turbine wakes. Fixed-wing uncrewed aerial systems (UAS) provided average wake profiles [8] and later on also revealed first tip vortices [9]. Easier to operate and more flexible in the deployment are multicopter UAS (also known as drones). They were used to investigate mean flow in the wake with single UAS [10], with a fleet of multiple UAS for multi-point, simultaneous measurements [11] and tip vortices [12]. In those studies, single instances of tip vortices were analysed and a systematic to derive circulation and core radius was developed. In this study, the goal is to analyze a larger database of measurements, develop a methodology to automatically detect the vortices and show that vortex decay can be plausibly measured with the DLR SWUF-3D fleet of UAS. In Sect. 2 we describe the experimental setup, in Sect. 3 the methodology is introduced and in Sect. 4 we show the results and analyzes of vortex measurements.

Table 1: Measurement flights on 24 July 2024

#	t	Ψ	Ψ'	Ψ''	U	TI	$\Delta\theta/\Delta z$
	UTC	deg	deg	deg	m s^{-1}	%	K/100m
53	24.07.2024 07:25	307	315	299	7.8	15	-0.2
54	24.07.2024 08:00	307	310	301	7.2	18	0
56	24.07.2024 09:10	306	310	302	7.1	18	0
58	24.07.2024 10:00	296	310	288	8.1	13	-0.2
60	24.07.2024 11:40	295	298	288	8.6	18	-0.1
61	24.07.2024 12:15	293	298	294	9.0	11	-0.1
62	24.07.2024 12:50	291	298	288	8.8	13	-0.3
63	24.07.2024 13:15	291	298	290	8.6	16	-0.25
64	24.07.2024 14:15	298	298	297	8.0	15	0.1
65	24.07.2024 14:35	298	298	294	8.1	15	0

2 Experiment and Instrumentation

2.1 Experimental setup

In July 2024, a campaign with the DLR SWUF-3D fleet was carried out at the Krummendeich research wind farm WiValdi. Details about the setup of the two turbine wind farm can be found at `https://windenergy-researchfarm.com/`. Meteorological observations at the site have been collected since 2020 [13] and the two wind turbines (OPUS1 and OPUS2) of type Enercon E-115 were installed in 2023 and are operating since then with some interruptions due to installation of sensors and testing.
During the two-week campaign we dedicated one day to wake measurements at wind turbine OPUS2 which at that day was subject to free inflow from north-westerly directions. Of 79 flights during the campaign, this comprises flight numbers 53–65. The ten flights listed in Tab. 1 were performed between 07:00 UTC and 15:00 UTC. The conditions were statically neutral atmospheric stability conditions at wind speeds from 7–10 m s^{-1} and turbulence intensities 10–20%. Static stability is determined from the potential temperature gradient $\Delta\theta/\Delta z$ within the rotor layer (34–141 m) as measured by an on-site microwave radiometer.

Ten drones were used during these flights to hover at fixed positions relative to the turbine. Five drones are positioned in the wake at 0.5 rotor diameters D downstream and a second row of five drones is positioned at 1 D. In the first flight (flight #53), drones were even positioned at 0.25 D downstream, but the crew decided to keep a safer distance to the turbine for the successive flights. For flights #62-65, an additional drone was programmed to fly continuous cross-sections in between the two lines of hovering drones at 0.75 D. Figure 1 shows a sketch of the setup. In the sketch, it is indicated how the projected wake based on wind turbine yaw angle Ψ before the flight differs from the measured wake with the wind direction Ψ'' as recorded during the flight. The orientation of the pattern Ψ' was changed twice during the day, turning it slightly further west due to the observations in the field. Both, wind direction and wind turbine yaw angle are not constant during the measurement flights, but vary with turbulent wind fluctuations.

2.2 Instrumentation

The type of drones that is used in this study is the Holybro QAV250 with a characteristic dimension (rotor tip distance) of 0.41 m and a weight below 0.7 kg. The main features of the system are described in Wetz et al. 2021 [14]. The wind algorithm is based on inertial measurements of the drone itself, calibrated seperately for the longitudinal and lateral wind components in wind tunnel measurements [15], and was later expanded to vertical wind [16] and fast-response temperature [17]. We showed in previous studies [18] that atmospheric turbulence can be resolved up to 2 Hz with the system. The resolution is mainly limited by noise due to vibrations which superimposes the low-energy small scale eddies. The system can provide data at higher resolution with raw data being sampled up to 250 Hz. We set the sampling rate for this study to 100 Hz but still apply an analog filter on acceleration data at 6 Hz. With this setup, tip vortices of wind turbines can be resolved while noise due to vibrations is filtered effectively.

3 Method

In this section we describe the methods to detect and quantify wind turbine tip vortices from in situ time series.

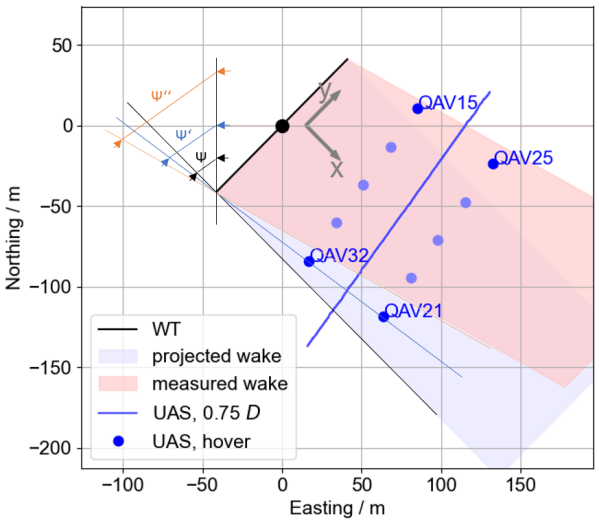

Figure 1: Sketch of the experimental setup with 10 UAS (blue dots) in the wake (blue shading for the projected wake for the UAS pattern and red for the measured wind direction) of the OPUS2 (black dot and line for rotor diameter) wind turbine for flight #64. The blue line shows the flight path of QAV18 with its continuous horizontal profile flight.

Table 2: Summary of conditions for automatic wake detection.

Description	Variable	Condition
Amplitude	Δu_x	>4 m s^{-1}
Ramp gradient	$\lvert\frac{\Delta u_y}{\Delta t}\rvert$	>10 m s^{-2}
Ramp direction	$\operatorname{sgn}\left(\frac{\Delta u_y}{\Delta t}\right)$	$-\operatorname{sgn} y$
Ramp duration	Δt	0.02 s$< \Delta t <$0.25 s

3.1 Wake vortex detection

We know from Wetz and Wildmann (2023) [11] that signatures of tip vortices can be seen in drone measurements if they hover at the edge of a wind turbine wake in a streamwise distance of less than one rotor diameter. These vortices rotate about a vertical axis at hub height and thus appear primarily in the horizontal wind components. A slight tilt of the vortex is expected due to the blade movement and the mean flow velocity [9], but is neglected in this study for simplicity. Wildmann and Kistner (2024) [12] showed that single vortices can be extracted and analyzed to quantify their characteristic features. For more systematic analyses, we now want to apply some automatic detection of vortices for a larger dataset of wake measurements at the WiValdi site. The drones record time series of streamwise and spanwise flow velocity during the hovering periods, which both show vortex features. For the vortex detection we only use the spanwise flow velocity because of a more distinct signal. In the spanwise velocity u_y, vortices are characterized by a change of sign which can be easily detected and filtered for the conditions that are listed in Tab. 2. The values are determined empirically to conservatively only detect clear vortex signatures.

Figure 2 shows an 8 s example of the time series of u_x and u_y for a hover flight. It shows two vortices with a separation of just below two seconds at $t \approx 67$ s and $t \approx 69$ s, which corresponds to the rotational speed of the rotor and successively produced tip vortices. A vortex which likely passed a bit further from the measurement point and is thus less pronounced in the data can be seen at $t = 65$ s. The latter is not detected with the automatic detection algorithm because the amplitude is too small. The right part of Fig. 2 shows a sketch of where the vortex passed the drone (dashed red line). We can read the location from the combination of u_x and u_y. The falling edge ramp defines the rotational direction, the positive u_x peak the side of the vortex and the fact that Δu_y is obviously greater than the amplitude of the peak in u_x suggests that the pass was inside the core radius.

After initial detection of vortices with this method, the next step is to derive vortex parameters.

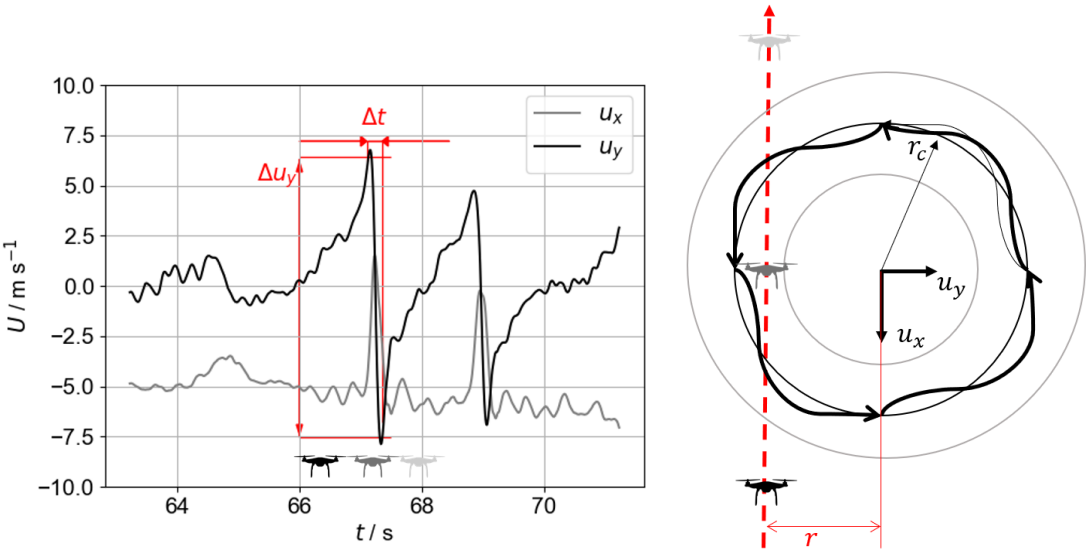

Figure 2: Left: Time series of u_x and u_y for an 8 s period with three vortices passing and description of the detected parameters Δu_y and Δt. Right: Sketch of the vortex with its coordinate system and the path where it passes the drone as a dashed red line. The grey-scaled drone icons on the left and the right illustrate the position relative to the vortex at the specific time.

3.2 Vortex models

In this study, we use the two vortex models Burnham-Hallock [19] and Lamb-Oseen [20]. As was shown in Wildmann and Kistner (2024) [12], we expect the Lamb-Oseen to be a better fit in the young vortex age and the Burnham-Hallock in the more developed vortex stage. The Lamb-Oseen model is used as described in Holzäpfel et al. (2000) [20]:

$$V_t(r) = \frac{\Gamma}{2\pi r}\left(1 - \exp\frac{-1.26r^2}{r_c^2}\right) \quad , \tag{1}$$

and the Burnham-Hallock model as:

$$V_t(r) = \frac{\Gamma}{2\pi r}\frac{r^2}{r^2 + r_c^2} \quad . \tag{2}$$

These two models will be used in parallel to fit measured time series of u_x and u_y and determine the vortex parameters associated to them.

3.3 Determine vortex parameters

In order to determine the vortex parameters Γ, r_c and the position of the vortex relative to the drone r_y, we fit the observed velocities in streamwise (u_x) and spanwise (u_y) direction to the model-values:

$$\alpha = \arctan\frac{y}{x} \tag{3}$$

$$\hat{u}_x = V_t(r)\cos\alpha \tag{4}$$

$$\hat{u}_y = V_t(r)\sin\alpha \tag{5}$$

Since V_t in Eq. 1 and 2 are functions of the vortex radius r, we need to convert the time series as measured by the drones to space using the Taylor hypothesis $x = \bar{U}t$. Determining the mean advection velocity of the vortices $\bar{U}$ is not straight-forward. Using the mean inflow velocity will yield an overestimation of the wake velocity. If we use the mean or median of the drone that measures the vortices, the value may be biased due to an instationary wake position that will have the drone measure partially inside and partially outside the wake. The simultaneous measurements with two rows of drones in 0.5 D

and 1 D, allows to use the cross-correlation function of the spanwise velocity of two streamwise separated drones to determine the advection time of the tip vortices, which yield a strong signal in u_y according to the following equations:

$$R(\tau) = \sum_{t=-T}^{T} u_{y,1}(t)\, u_{y,2}(t-\tau) \tag{6}$$

$$\tau_{max} = \underset{\tau}{\operatorname{argmax}}\, R(\tau) \tag{7}$$

Figure 3 shows the correlation function between the drones QAV32 & QAV21 (red curves) and QAV15 & QAV25 (green curves) with the highlighted corresponding maxima of correlation at τ_{max} (red and green dots) for all flights.

In the last step, the time lag can be converted to advection speed with the constant distance between the drones, i.e. $D/2$:

$$\bar{U} = \frac{0.5D}{\tau_{max}} \tag{8}$$

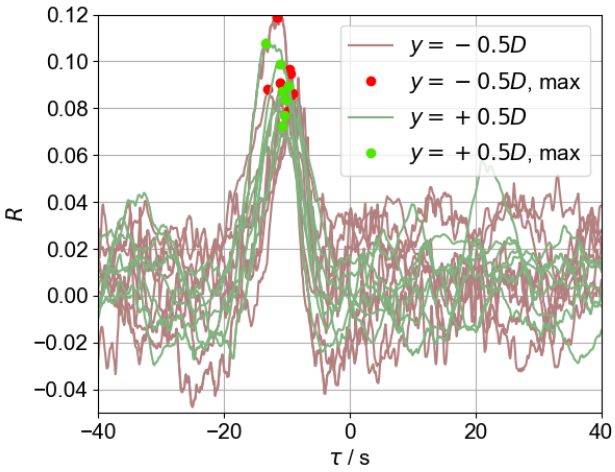

Figure 3: Cross-correlation functions of u_y of streamwise separated drones at positions $y = +0.5D$ (green) and $y = -0.5D$ (red). The dots indicate the detected maxima that is used for calculation of advection velocity.

Having converted the time series into a space series, we perform a minimization of the objective error function, which is defined as the sum of error of the two velocity components u_x and u_y:

$$\epsilon = \sigma_{\epsilon,x} + \sigma_{\epsilon,y} \quad , \tag{9}$$

where the difference between model and measurement is calculated as its variance:

$$\epsilon_x = \hat{u}_x - u_x \qquad \epsilon_y = \hat{u}_y - u_y \tag{10}$$

$$\sigma^2_{\epsilon,x} = \frac{1}{n-1}\sum_{i=1}^{n}(\epsilon_{x,i} - \overline{\epsilon_x})^2 \qquad \sigma^2_{\epsilon,y} = \frac{1}{n-1}\sum_{i=1}^{n}(\epsilon_{y,i} - \overline{\epsilon_y})^2 \tag{11}$$

Empirically, we determined to get best results for fitting the vortex models, when a time period of 0.5 s before and after the vortex center (zero crossing of u_y) is used as input for the optimization algorithm in order to avoid the influence of previous and following vortices in the analyzed time series.

3.4 Normalization

For comparability of the results to models and wind tunnel studies, we can normalize the vortex parameters. For the circulation, we calculate an initial vortex strength as

$$\Gamma_0 = \frac{\pi U_\infty^2 C_t}{\Omega N_b} \quad , \tag{12}$$

from the thrust coefficient C_t, the inflow velocity U_∞, the rotor speed Ω and the number of blades $N_b = 3$. This equation is only a rough approximation according to [1], which assumes a constantly loaded rotor. We also just use an approximation of C_t which is derived from measured inflow velocity U_∞ and produced power P averaged over the flight periods. We numerically determine the axial induction factor a from the equation

$$P = 2\rho A U_\infty^3 a(1-a)^2 \quad , \tag{13}$$

with rotor-swept area A and air density ρ. Then, we calculate thrust T and C_t according to:

$$T = \frac{1}{2}\rho A U_\infty^2 \cdot 4a(1-a) \tag{14}$$

$$C_t = \frac{T}{\frac{1}{2}\rho A U_\infty^2} \tag{15}$$

$$\tag{16}$$

We do not have a value for the initial core radius. In this study we want to primarily show relative differences so that we use the average determined core radius $\overline{r}_{\mathrm{c,lf}}$ at $[x, y] = [0.5, -0.5]D$ to scale all other values. U_∞ is taken from sonic anemometer measurements at the inflow mast which is about 600 m West of OPUS2.

4 Results

4.1 Wind speed deficit and turbulence in the wake

Averaging the hover flights and plotting the results over the y-axis along with the continuous measurements of the profiling drone, a comprehensive quantification of the horizontal wind distribution in the wake can be obtained as shown in Fig. 4

It shows that the location of the wake was well met with the drone setup. The variability of the flow is larger in the negative y-direction (downward blade motion) and the drones are located more directly in the area of tip vortices. The vertical component in this study, in contrast to the description in [16], was calibrated to provide absolute values and shows that the profiling as well as the hovering drones can well capture the three-dimensional dynamics of the wake with its rotational characteristics. A clear difference between vertical velocity on the two sides of the rotor is evident. An upward motion of the air in negative y-direction and curiously almost zero vertical velocity on the other side is observed by the continuous profile at 0.75 D as well as the hovering drones at 0.5 D and 1 D. The accuracy of the absolute vertical velocity as measured by the drone is however still under investigation.

4.1.1 Goodness of fit for vortex models Figure 5 shows an example of a detected vortex with the two velocity components u_x and u_y in blue and the corresponding fits for Lamb-Oseen model (left) and Burnham-Hallock model (right) in red. Approximately 300 single instances of vortex measurements were analyzed and allowed an estimation of the vortex parameters, most of them by QAV32 at position $[x, y] = [0.5, -0.5]D$.

The question if the Lamb-Oseen or the Burnham-Hallock model should be used for the determination of vortex parameters can be ivestigated by looking at the magnitude of the error function value ϵ for the different measurement positions (see Tab. 3). It shows that the Lamb-Oseen model provides a slightly better fit on average. The overall differences are however small, which also shows in the differences between the determined values for circulation and core radius with the two models.

4.2 Wake vortex characteristics

To evaluate wake dynamics from the drone observations we show the normalized values of Γ (Fig. 6) and r_c (Fig. 7) over time for the four corner drones in the flight pattern and all available flights. It is obvious that most vortex detections were possible by QAV32 at the position $[x, y] = [0.5, -0.5]D$. This maybe due to the fact that this drone was best located at a position where the vortices were passing through.

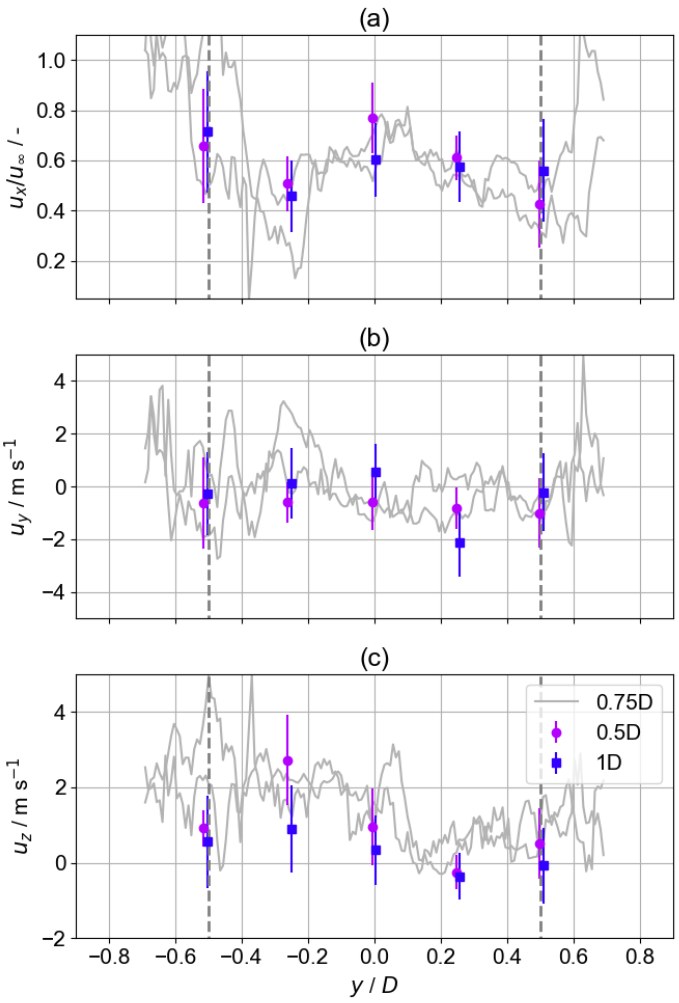

Figure 4: streamwise (a), spanwise (b) and vertical (c) velocity as measured by drones hovering in 0.5 D (pink) and in 1 D, as well as by the horizontal profiling drone in 0.75 D.

It could however also be an indication that vortices are more stable on that side of the wake due to the interaction with atmospheric shear and turbulence. Numerical simulations with actuator line model [4] as well as rotor-resolving RANS simulations [21] show this asymmetry of the wake for sheared inflow, but the parameters in the simulation are too different for a direct quantitative comparison. Performing comparable simulations with LES is planned as a next step. Further downstream and at the positive y-direction side of the wake (upward blade motion), scatter of the observations is significantly larger. However, on average, the circulation is very similar at all location as summarized in Tab. 4. There is a small decay of circulation with distance, whereas the core radius increases slightly. This is in accordance with theory that core radius increases proportional to the square-root of time $\frac{r_c}{r_{c,0}} \propto \sqrt{\frac{\nu t}{r_{c,0}^2}}$[22]. With only two measurement points along the x-axis, we can however not validate the relationship quantitatively.

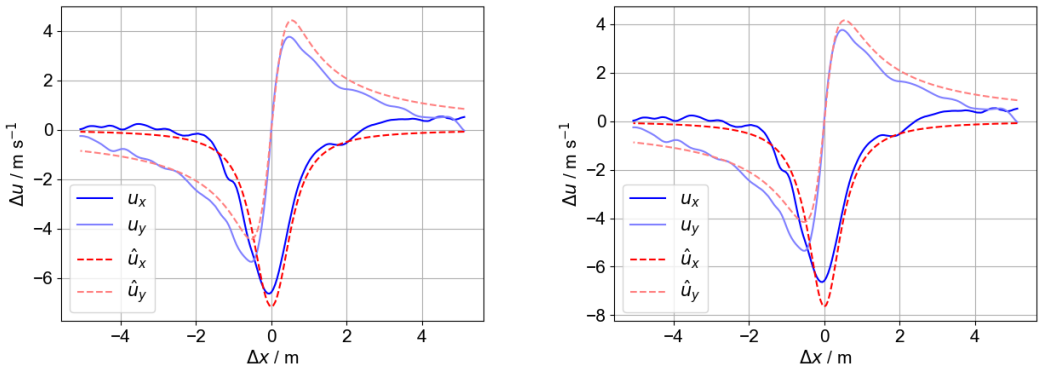

Figure 5: Examples of measurements of u_x (dark blue) and u_y (light blue) and the associated model fits (red) for Lamb-Oseen model (left) and Burnham-Hallock model (right).

Table 3: Average error function output for different positions and vortex models.

Vortex model	0.5 D ϵ / m^2 s^{-2}	-0.5 D ϵ / m^2 s^{-2}	1 D ϵ / m^2 s^{-2}	-1 D ϵ / m^2 s^{-2}
Burnham-Hallock	0.898	0.861	1.001	0.922
Lamb-Oseen	0.869	0.84	0.978	0.914

5 Discussion and Outlook

This study has demonstrated the feasibility of using a fleet of multicopter drones (SWUF-3D) to characterize wind turbine tip vortices in situ. Across ten flights, more than 300 vortices were successfully observed by four drones positioned at the outer edges of the flight pattern, with a concentration of detections at the 0.5 D downstream location in the negative y-direction. Analysis of these observations, yielding values for circulation (Γ) and core radius (r_c), provided insights into both wake dynamics and the capabilities of the measurement methodology. While the fitting of observations to the vortex model is subject to inherent uncertainties—likely due to the simplification of a 3D vortex to a 2D analysis and the neglect of vortex inclination—the approach proved effective. Notably, the use of spatially separated drones offered a unique opportunity to determine the tip vortex advection velocity via cross-correlation analysis, though the assumption of a constant velocity for each flight introduces another source of uncertainty given the variability of the incoming flow. The observed scatter in derived vortex parameters underscores the complex nature of the near-wake flow, particularly under high turbulence intensities. Indications of the expected increase in core radius with downstream distance (and thus vortex age), consistent with existing literature, were found in the experiment. However, the scatter of individual values and thus the uncertainty of the results, especially at 1 D is significant and further analyses are required.

With the now-established methodology for determining wake parameters from drone fleet observations, future work will focus on expanding the dataset through additional flights, enabling a more comprehensive analysis of the dependencies of wake decay on ambient turbulence and wind turbine operating conditions. Comparisons with more established wind measurements by sonic anemometers at an array of masts which is unique for the WiValdi site can be pursued in future to validate the accuracy of vortex parameter estimation. To further enhance vortex capture, future drone deployments will explore positioning the drones slightly further outside the initially projected wake boundaries. Measuring at a greater number of streamwise distances is also planned to facilitate the development and validation of more robust vortex decay models. Furthermore, the acquired measurement data will be used to analyze, validate, and improve

Table 4: Average values for wake parameters for different positions and vortex models.

Parameter	0.5 D	-0.5 D	1 D	-1 D
Γ/Γ_0	0.74	0.68	0.39	0.42
$r_0/r_{0,c}$	1.19	1.0	1.12	1.04

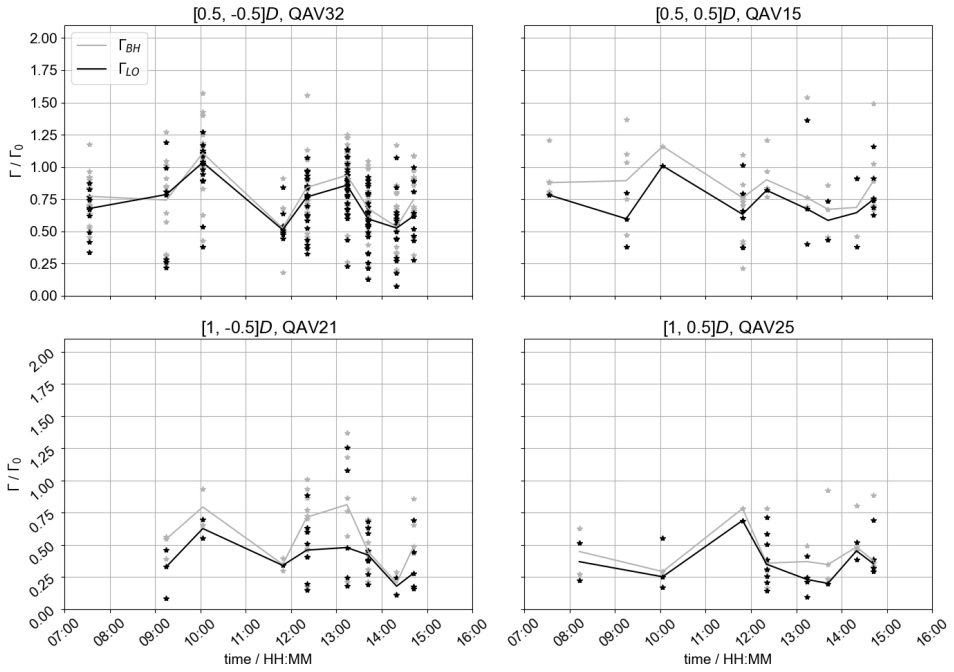

Figure 6: Normalized measured circulation Γ/Γ_0 over time for all flights. The dots show each individual vortex, the lines connect the median values. Both, BH (grey) and LO (black) model fits are shown. The top row shows the $0.5D$ streamwise distance, the bottom row the $1D$ distance. Left is negative y-direction and right is positive.

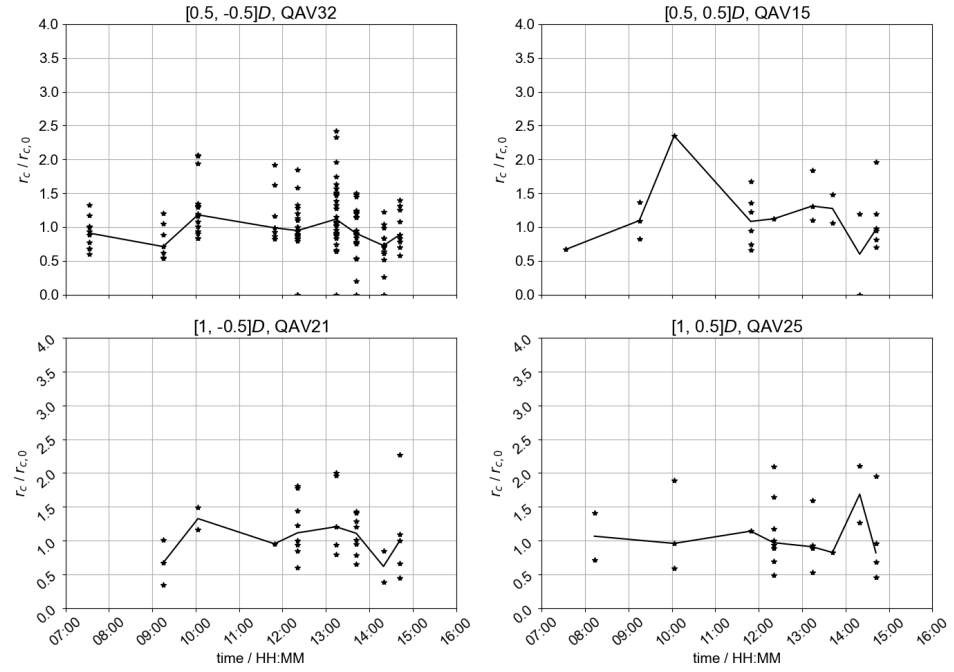

Figure 7: As Fig. 6, but showing normalized core radius $r_c/r_{c,0}$.

numerical simulations, building upon previous work such as that presented in [21]. Given the ongoing field experiments investigating active wake control strategies through pitch control [23], future drone measurements offer the potential to directly validate the effects of these control strategies on tip vortex behavior in situ. Further drone experiments at the WiValdi test site were conducted in spring 2025, providing an even larger database to pursue these research directions.

Acknowledgements
This research has been supported by the HORIZON EUROPE European Research Council (grant no. 101040823, ESTABLIS-UAS). This work was also partly accomplished within the research project Near-Wake. We greatly acknowledge the financial support of the German Federal Ministry for Economic Affairs and Climate Action, through FKZ 03EE3097B, that enabled this work.
The authors acknowledges the use of a large language model (e.g., Gemini and llama3.2) for language improvements. We acknowledge internal review and advice by Thomas Gerz and Frank Holzäpfel. Many thanks to Almut Alexa and Laszlo György for the hard work in the field to collect data with the UAS fleet.

References

[1] Sørensen J N, Mikkelsen R, Sarmast S, Ivanell S and Henningson D 2014 *Journal of Physics: Conference Series* **524** 012155

[2] Neunaber I, Hölling M and Obligado M 2024 *Renewable Energy* **223** 119935 ISSN 0960-1481

[3] Ivanell S, Mikkelsen R, Sørensen J N and Henningson D 2010 *Wind Energy* **13** 705–715

[4] Kleusberg E, Benard S and Henningson D S 2019 *Wind Energy* **22** 1789–1799

[5] Bartl J, Hansen T H, Kuhn W L, Mühle F and Sætran L 2020 *Journal of Physics: Conference Series* **1669** 012027

[6] Mühle F, Bartl J, Hansen T, Adaramola M S and Sætran L 2020 *Wind Energy* **23** 1286–1300

[7] Soto-Valle R, Cioni S, Bartholomay S, Manolesos M, Nayeri C N, Bianchini A and Paschereit C O 2022 *Wind Energy Science* **7** 585–602

[8] Wildmann N, Hofsäß M, Weimer F, Joos A and Bange J 2014 *Adv. Sci. Res.* **11** 55–61

[9] Mauz M, Rautenberg A, Platis A, Cormier M and Bange J 2019 *Wind Energy Science* **4** 451–463

[10] Li Z, Pu O, Pan Y, Huang B, Zhao Z and Wu H 2022 *Sust. E. Tech. and Ass.* **53** 102537 ISSN 2213-1388

[11] Wetz T and Wildmann N 2023 *Wind Energy Science* **8** 515–534

[12] Wildmann N and Kistner J 2024 *Journal of Physics: Conference Series* **2767** 042004

[13] Wildmann N, Hagen M and Gerz T 2022 *Journal of Physics: Conference Series* **2265** 022029

[14] Wetz T, Wildmann N and Beyrich F 2021 *Atm. Meas. Tech.* **14** 3795–3814

[15] Kistner J, Neuhaus L and Wildmann N 2024 *Atmospheric Measurement Techniques* **17** 4941–4955

[16] Wildmann N and Wetz T 2022 *Atm. Meas. Tech.* **15** 5465–5477

[17] Wildmann N and György L 2025 *EGUsphere* **2025** 1–20

[18] Wetz T and Wildmann N 2022 *Journal of Physics: Conference Series* **2265** 022086

[19] Burnham D C and Hallock J N 1982 *US. Dept. of Transp. Fed. Av. Adm., Tech Report* **4** 590–599

[20] Holzäpfel F, Gerz T, Frech M and Dörnbrack A 2000 *Journal of Aircraft* **37** 1001–1007

[21] Imiela M, Wrba L, Probst A, Bangga G and Englberger A 2024 *Journal of Physics: Conference Series* **2767** 022009

[22] Holzäpfel F 2004 *AIAA Journal* **42** 1369–1377

[23] Brown K, Houck D, Maniaci D, Westergaard C and Kelley C 2022 *AIAA Journal* **60** 3298–3310